Astronomical and Astrophysical Transactions (*AApTr*), 2016, Vol. 29, Issue 4, pp. 547–556,
ISSN 1055-6796, Photocopying permitted by license only, ©Cambridge Scientific Publishers

Type II radio bursts in cycles 23 and 24

I.A. Bilenko*

Lomonosov Moscow State University, Sternberg Astronomical Institute, Moscow 119991, Russia

Received 15 September, 2015

An analysis have been made of the all type II radio bursts (RBIIs) observed in cycles 23–24 from 1995 to 2014. The number of RBIIs is greater during the maximum of cycle 23 than in minima of cycles 23 and 24, but neither their number nor their parameters revealed univocal correspondence with the Wolf numbers. Some local increases in RBII number coincide with increases in Wolf numbers and others are associated with the decreases in Wolf numbers. The distribution of RBIIs reveals the dependence on the evolutionary changes of the solar global magnetic field (GMF). RBIIs can be separated into two classes depending on the RBII end frequency. The cycle evolution and parameter interrelations are different for the RBIIs of different classes. There is no unambiguous dependence between the RBII parameters. The interrelations between the different class RBII parameters are also different. All interrelations between RBII parameters are non-linear and are fairly widespread. RBIIs are also separated into three groups depending on the GMF strength.

Keywords: Sun: radio radiation – Sun: magnetic fields – Sun: activity

1 Introduction

The investigation of type II radio bursts (RBIIs) and regularities in their generation and distribution is a critical task in the modern physics of the solar atmosphere, because of their association with shock waves generated during solar eruptive events and, consequently, their connection to the coronal mass ejections (CMEs) that determine the space weather at the Earth's orbit.

Payne-Scott et al. (1947) were the first who identified RBII, then Wild and McCready (1950) classified them as RBII. The dynamic spectrum of RBII shows slowly drifting emission bands from high to low frequency. They often have complicated fine structure (Korolev 1974, Chernov 2007). RBIIs are often identified with fundamental and harmonic plasma emission bands. Sometimes the emission is also band-split (Vrsnak et al. 2001). It is widely assumed that RBIIs are the manifestation of magnetohydrodynamical shock waves propagating in the solar atmosphere with velocities

*Email: bilenko@sai.msu.ru

above Alven speed. Plasma electrons accelerated by the shock waves generate Langmuir waves, which are transformed into radio waves at the approximately local plasma frequency or its harmonics (Melrose 1980). The shock wave generation mechanism is not yet fully understood.

Alternatively, it was proposed that RBIIs could be the result of synchrotron radiation from high energy electrons. Kuckes and Sudan (1971) proposed the model of RBII generation by coherent synchrotron deceleration of 100 keV electrons. Pohjolainen et al. (2013) founds that in most cases (in 18 out of 25 events) RBIIs were associated with the CME leading edge, but 7 events could have a synchrotron source.

Many theories consider the RBII as the result of fast-propagating CMEs producing shock waves (eg., Gopalswamy et al. 2009), CMEs and coronal loops (Cho et al. 2013). It is commonly assumed that RBII are the result of plasma radiation from Langmuir waves excited by suprathermal electrons in a shock wave driven by a fast CME. RBII are also associated with flares (Dodge 1975, Vasanth and Umapathy 2014) or with EUV waves (Cunha-Silva 2015). High correlation was found between RBII and solar energetic particle events (Gopalswamy et al. 2008). But in some papers (e.g. Dodge 1975, Vrsnak et al. 2006, Cho et al. 2007, Bastian 2007) it was shown, that the calculated RBII speeds and heights do not correspond to the observed CME speeds and heights. Moreover, some fast CMEs are not associated with RBII (Sheeley et al. 1984). Furthermore, Nitta et al. (2014) showed that neither EIT waves (large-scale coronal propagating fronts) nor RBIIs by themselves serve as necessary conditions for coronal shock waves. Vasanth and Umapathy (2014) found that the parameters of DH RBIIs associated with flares and CMEs did not depend on the time of appearance in the solar cycle 23. They noted that there were no differences in such properties of RBII as start frequency and end frequency between the cycle 23 rise phase events and decay phase events. Of more than about 20000 CMEs, observed during 1995–2014, only about 300 were associated with RBIIs. CMEs with the same parameters and occurred under the same conditions can be radio-loud (associated with a RBII) or radio-quiet (without RBII). During the same time, over hundreds of thousands of flares were observed. All this suggests that by themselves, neither CMEs nor flares are the source of RBIIs.

The investigations revealed that the cycle evolution changes in the global magnetic field (GMF) influence on the CMEs (Bilenko 2012, 2014) and on the distribution of RBII associated with CMEs (Bilenko 2014). The analysis of RBIIs associated with CMEs showed that the RBIIs tend to occur when the long-lived large-scale structures existed during the sector global magnetic-field (GMF) structure domination.

Thus, it is important to study the cycle behavior of all RBII observed by Wind/WAVES and STEREO missions from 1995 to 2014. Additionally, the analysis of RBII may reveal some information on the physical conditions favorable for the generation of RBIIs.

2 Data

A set of 650 DH RBII listed in the Wind/WAVES and STEREO (Bougeret et al. 1995, 2008) catalog observed during 19952014 in cycles 23 and 24 are used in the present analysis. The frequency range of RBII is from 20 kHz to 14 MHz for Wind/WAVES

RAD1 and RAD2 data and from 20 kHz to 16 MHz for STEREO data. The observed DH wavelength corresponds to the heights of ≈2–10 solar radii.

To compare RBII with the solar GMF evolution we used calculation results on coronal magnetic fields from the Wilcox Solar Observatory (WSO) for years 1995–2014 (Altschuler 1969, 1075, 1977, Hoeksema 1984, 1986).

Data on Wolf sunspot numbers were taken from the National Geophysical Data Center (USA).

3 Type II radio burst parameters in cycles 23 and 24

In Fig. 1a, the magnetic-field strength evolution from the calculated source-surface longitudinal GMF distribution diagram (Bilenko 2012, 2014) is presented. Coefficient Klon is shown in Fig. 1b. Klon describes the GMF structure cycle changes (Bilenko 2012, 2014). The amplitude of Klon is minimal during the periods of quasi-stable GMF, when large long-lived two-polarity magnetic structures existed and the amplitude of Klon is maximal during the periods of the fast GMF structure reorganization.

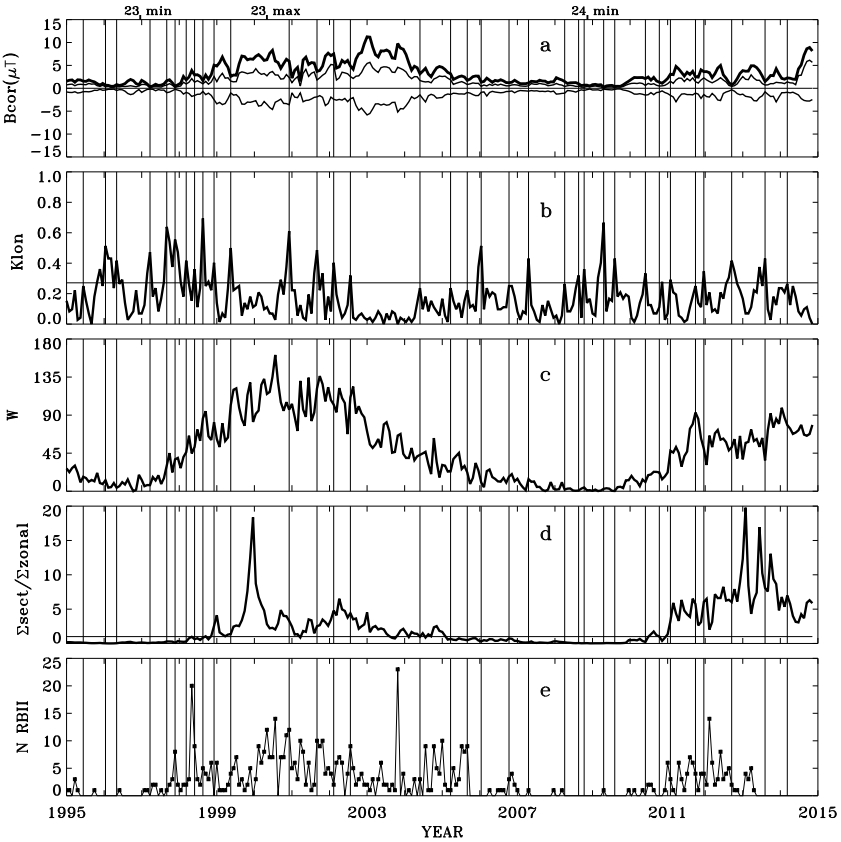


Figure 1 (a) magnetic-field strength; (b) K_{lon}; (c) Wolf number evolution; (d) the ratio of the sectoral harmonic sum to the zonal harmonic sum; (e) CR-averaged RBII rate.

The CR-averaged daily Wolf number evolution is displayed in Fig. 1c. Figure 1d shows the ratio of the sectoral harmonic sum to the zonal harmonic sum derived from the spherical decomposition of the synoptic coronal magnetic-field maps calculated using PFSS model. The horizontal line marks the level where the sum of the sector harmonics is equal to the sum of the zonal harmonics. The CR-averaged RBII rate is shown in Fig. 1e. Thin vertical lines denote the GMF structure reorganizations, the peaks in Klon. The 2σ (Klon = 0.27) level was used. This level corresponds to the significant changes in the structure of the GMF. The maximum and the minima of cycles 23 and 24 are marked at the top of Fig. 1.

From Fig. 1 we can see that the number of RBII is sharply increased during the sector structure domination. During the periods of zonal structure domination, their number is minimal. In some periods the Sun exhibits a global reconfiguration of magnetic fields which has its effects in large-scale processes in the solar atmosphere. The fast global changes of the solar magnetic fields, accompanied by the rapid coronal magnetic-field structure reconfiguration and decrease in magnetic-field strength have an influence on the rate of CMEs, prominence eruptions and their parameters (Bilenko 2012, 2013, 2014).

In Fig. 1e, we can see that the CR-averaged rate of RBII is lower during the periods of the GMF reorganizations. It is interesting to note that the majority of RBII are concentrated in the periods of quasi stable GMF. They tend to occur when the GMF structure is quasi stable (between the vertical lines which mark the GMF reorganization). This is especially clearly seen during the growth phases of cycles 23 and 24 and the decline phase of cycle 23. A similar result was revealed for RBIIs associated with CMEs (Bilenko 2015). During solar maximum some local increases in RBII rate coincide with GMF reorganizations. The magnetic-field strength is lower during times of the GMF reorganizations and higher when the GMF structure is stable. It is considered that the majority of RBIIs are generated during CMEs. But CMEs have different parameters, depending on the stable or changing GMF structure (Bilenko 2014). This indicates that RBIIs can occur under different conditions in the solar atmosphere. The comparison with Wolf numbers, which manifest the local, active region (AR), magnetic field cycle evolution, shows, that RBII did not follow Wolf numbers uniquely. In some CRs local increases in RBII coincide with increase in Wolf numbers and in other CRs they are associated with the decrease in Wolf numbers. So, a number of RBIIs can be associated with CMEs that result from active processes in ARs, and some RBIIs – with CMEs that result from GMF structure reorganization. These CMEs have different parameters and different cycle distribution. The increases in RBII rate in 2003.8 and during 2004.5–2006 are not associated with any increases in Wolf number, but they coincide with the increases in the GMF strength (Fig. 1a). They also coincide well with increases in the rate of CMEs associated with GMF structure reorganization (Bilenko 1014). The comparison of the cycle evolution of the GMF and local magnetic fields (Fig. 1a, c) shows that they are different. The difference in the local and global magnetic fields in different cycles was studied in detail in Makarov, Sivaraman (1989), Makarov et al. (2001). They suggested the leading role of the GMF. The GMF strength is lower in cycle 24 compared to that in cycle 23.

In Fig. 2 the RBII parameter cycle evolution is presented for 1995–2014. The parameters of each PBII are shown in Fig. 2(a–e) and that of CR averaged in Fig. 2(k–o).

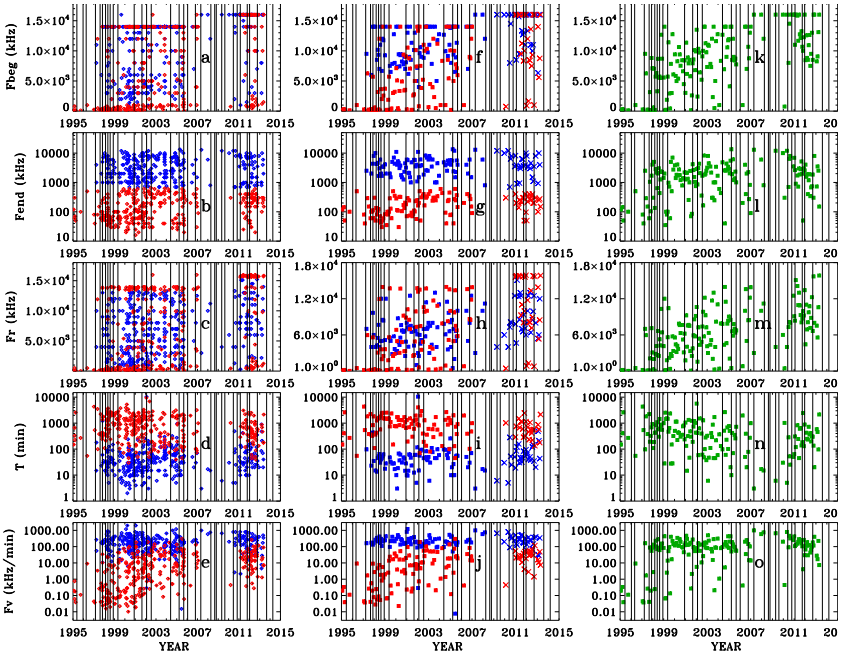


Figure 2 RBII parameters. The start frequency, Fbeg (a), end frequency, Fend (b), the difference between the starting and ending frequencies, Fr (c), duration, T (d), the drift velocity, Fv (e) for each PBII; (f–j) that of CR averaged for P1 (red) and P2 (blue); (k–o) that for total CR averaged. Squares denote cycle 23 and crosses – cycle 24.

In Fig. 2(f–j) the CR-averaged RBII parameters for P1 and P2 are displayed. Thin vertical lines denote the GMF structure reorganizations, the same as in Fig. 1. From Fig. 2 it is seen that the RBIIs may be separated in two classes depending on the end of their frequency, which also determines the frequency range, duration, and drift rate of a RBII.

Figure 3(a) presents the histogram of the Fend of all RBIIs. Thin vertical line denotes the median of Fend, the criterion for periods P1 and P2. Figure 3(b) shows the total RBII rate and Fig. 3(c, d) the rate of P1 and P2 RBIIs. The rate of P2 RBII is more uniform during cycles 23, 24, and P1 RBII rate reveals a more prominent cycle dependence.

The total and CR-averaged P1 PBII start time began to increase from 1998, peaked in ≈2004 and then decreased (in Wind/WAVE data). Cycle 24 RBIIs have on average higher start frequency, which is due to the higher STEREO frequency detection level. P2 PBII start time remained, on average, on the same level (Fig. 2(a, f, k)). The start frequency corresponds to the height at which a RBII is detected (Gopalswamy 2005). The Fend of total and P1 RBIIs had maximum in ≈2005 and that of P2 RBIIs slightly decreased from 1995 to 2014 (Fig. 2(b, g, l)). Fr is greater in cycle 24 due to the STEREO data (Fig. 2(c, h, m)). The duration (T) of P1 RBIIs decreased from 1995 to 2008, but the duration of P2 RBIIs increased from 1995 to 2003.5, and then decreased to the cycle 24 minimum. In cycle 24 the duration of both populations did not show cycle phase dependence (Fig. 2(d, i, n)). RBIIs are

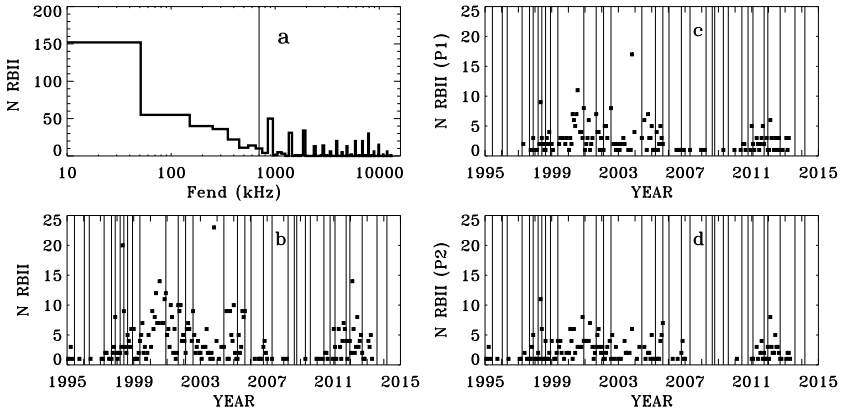


Figure 3 The histogram of the Fend (a); total RBII rate (b); the rate of P1 RBIIs (c); the rate of P2 RBIIs (d).

Table 1 Statistics of RBII parameters.

	Fbeg (kHz)	Fend (kHz)	Fr (kHz)	T (min)	Fv (kHz/min)
			Total		
Mean (kHz)	8.7×10^3	2.1×10^3	6.53×10^3	1.6×10^5	$1. \times 10^2$
Median (kHz)	1×10^4	7×10^2	6×10^3	1.19×10^2	46.42
Variance	3.6×10^7	8.8×10^6	2.8×10^7	1.7×10^{13}	5.08×10^4
STD	6×10^3	2.96×10^3	5.3×10^3	4.13×10^6	225.4
MAD	5.6×10^3	2.3×10^3	4.72×10^3	3.24×10^5	142.25
Skewness	−0.24	1.61	0.23	25.37	2.41
Kurtosis	−1.64	1.60	−1.34	642.94	1949
			Period 1 (P1)		
Mean (kHz)	10.8×10^3	4.0×10^3	6.78×10^3	3.17×10^5	238.41
Median (kHz)	1.4×10^4	2.9×10^3	7×10^3	34.92	166.93
Variance	2.4×10^7	1×10^7	1.6×10^7	3.32×10^{13}	6.44×10^4
STD	4.8×10^3	3.2×10^3	4.1×10^3	5.76×10^6	253.83
MAD	4.4×10^3	2.7×10^3	3.5×10^3	6.31×10^5	173.35
Skewness	−0.68	0.83	0.13	18.08	2.87
Kurtosis	−1.13	−0.41	−1.17	326	13.4
			Period 2 (P2)		
Mean (kHz)	6.5×10^3	1.96×10^2	6.3×10^3	1.04×10^3	19.71
Median (kHz)	4×10^3	1.2×10^2	3.6×10^3	6.59×10^2	4.37
Variance	4×10^7	2.8×10^4	4×10^7	1.2×10^6	1.4×10^3
STD	6.3×10^3	1.66×10^2	6.3×10^3	1.1×10^3	37.47
MAD	6×10^3	1.39×10^2	5.9×10^3	8.12×10^2	23.26
Skewness	0.34	0.87	0.35	2.56	3.64
Kurtosis	−1.66	−0.39	−1.65	12.4	17.5

frequency drifting radio emissions. The drift rates reflect the decreasing density in the solar atmosphere. The plasma frequency changes as $Fp = 8.978 \times 10^3 \sqrt{N_e}$ (where Fp is in Hz and electron density N_e in cm^{-3}). The drift velocity (Fv) of P1 RBIIs

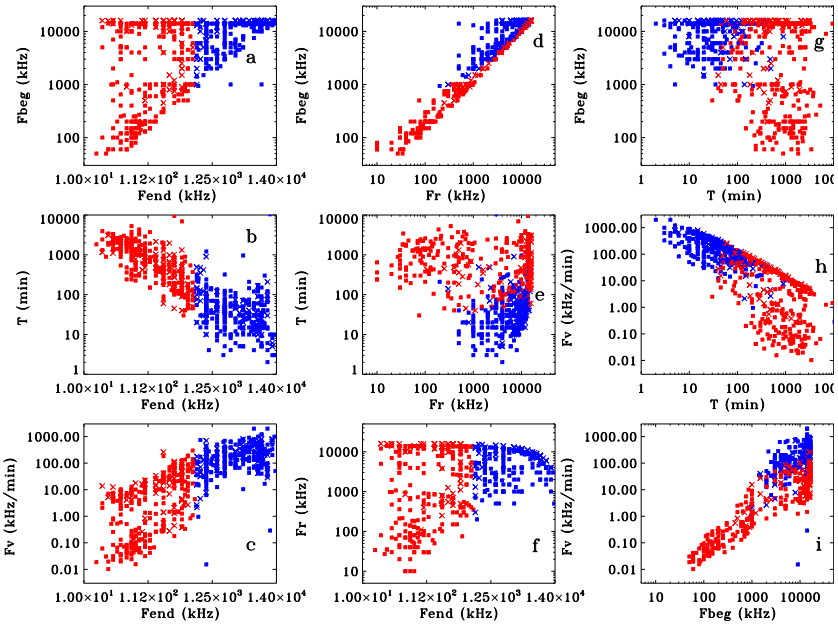


Figure 4 Interrelations between PBII parameters.

increased from the cycle 23 minimum to maximum and remained on that level in cycle 24. The drift velocity of P2 RBIIs was on the same level from 1995 to 2014, showing neither cycle nor cycle phase variations. It should be noted, that despite the average regularities, described above, each RBII parameter has a wide range of values.

The statistics of RBII parameters, such as mean, median, mean absolute deviation (MAD), variance, standard deviation (STD), skewness, and kurtosis for all RBII and that of P1 and P2 periods were calculated (Table 1). All parameters have non-normal distributions.

Figure 4 presents the interrelations between PBII parameters. The color code and symbols are the same as in Fig. 2. All interrelations are non-linear. Between parameters there is no-one correspondence. P1 RBIIs and P2 RBIIs behave in a different way. P2 RBIIs have, in general, lower duration time but wider Fr, higher Fv and Fbeg than P1 RBIIs. P1 RBIIs are separated into two subclasses (Fig. 4(a, c, f, g, h)). All dependences are fairly widespread. It is known that the frequency of a burst is a function of the plasma density in the RBII generation region so it means that RBIIs with the same parameters can be produced in the solar atmosphere regions under absolutely different plasma conditions.

4 Dependencies of type II radio burst parameters from the solar global magnetic field

In Fig. 5, the dependencies of CR-averaged P1 and P2 PBII parameters (a–e) and total CR-averaged parameters (g–k) *versus* MFlon and that *versus* Klon ((m–q) and

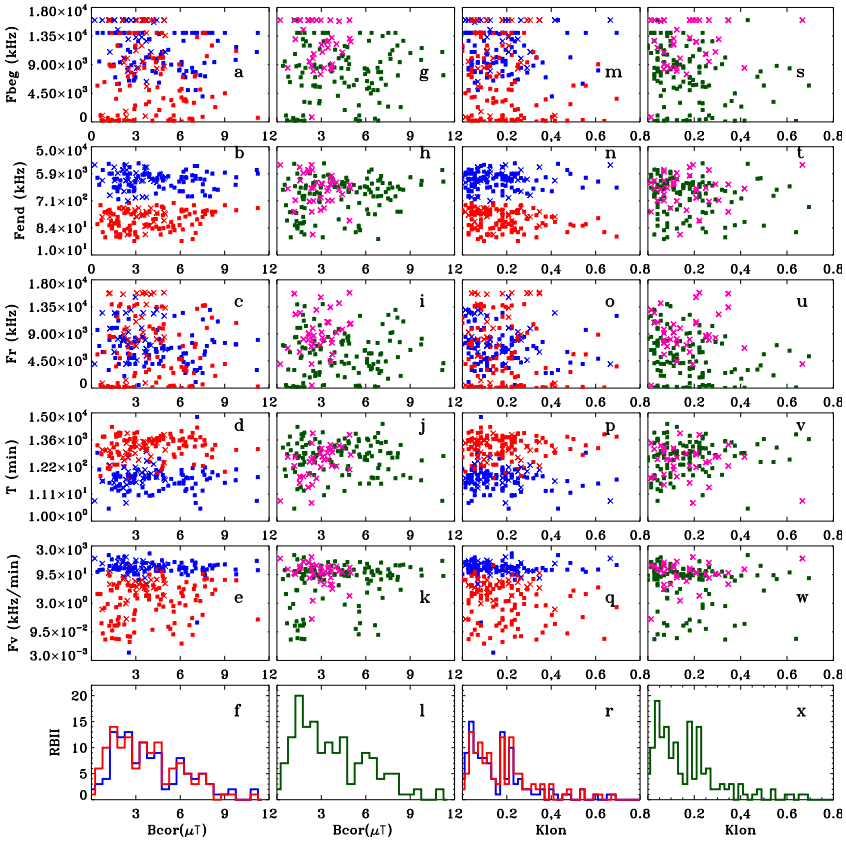


Figure 5 (a–e) dependencies of CR-averaged PBII parameters *versus* MFlon; (f–h) dependencies of CR-averaged PBII parameters *versus* Klon.

(s–w)) are shown. The corresponding histograms are presented in Fig. 5(f, l, r, x). The color code and symbols in Fig. 5(a–e) and (m–q) are the same as in Fig. 2. In Fig. 5(g–k) and (s–w) the CR-averaged RBIIs for cycle 23 an 24 are indicated by the color and symbol code: green-squares for cycle 23 and lilac-crosses for cycle 24. In histograms, Fig. 5(l, x) the overall 23 and 24 cycle CR-averaged data are presented. The histograms revealed different groups of RBII depending on the GMF strength. P1 and P2 RBIIs histograms are almost identical. RBIIs fall into three types depending on the GMF strength. The first type RBIIs are associated with magnetic fields in the range of ≈0–2.5 μT, the second type RBIIs are associated with the GMF in the range of ≈3.5–5 μT, and the third type RBIIs are associated with the GMF in the range of ≈5.5–8.5. Cycle 24 RBIIs are concentrated to the 0–5 μT GMF. In general, the histograms in Fig. 5(f, l), RBII number *versus* MFlon, match well that of CMEs (Fig. 5 in Bilenko 2014).

The histograms in Fig. 5(r, x), RBII number *versus* Klon, reveal two groups of RBIIs. The majority of RBIIs concentrate to low Klon ≈0–0.15 and ≈0.2–0.3. So, RBII occurs more frequently during the stable GMF. The population of RBII associated with high Klon (Klon $\geq$ 0,27, that is 2σ level), the periods of the GMF

reorganization, is not very rich, but clearly seen. During the reorganization periods of the GMF the number of RBIIs sharply decreased, but RBIIs have high Fv, long duration, not wide Fr, and moderate Fbeg.

5 Conclusion

An analysis has been made of the all RBII observed in cycles 23–24 from 1995 to 2014. According to the study, although the number of RBIIs is greater during the maximum of cycle 23 than in minima of cycles 23 and 24, neither their number nor their parameters revealed univocal correspondence with the Wolf numbers. In some CRs local increases in RBII number coincide with increases in Wolf numbers and in other CRs they are associated with the decreases in Wolf numbers.

RBII rate varies quite randomly, but most of the RBII tend to occur in periods between the GMF reorganizations, during the periods of quasi-stable GMF structure. This is more pronounced during the declining phase of cycle 23 from 2003 to 2009 and during rising phases of the cycles 23 and 24 from 1997 to 1999 and from 2010 to 2011. A similar result was revealed for RBIIs associated with CMEs (Bilenko 2015). This suggests that the RBIIs associated with the CMEs are not a separate class of RBIIs.

The distribution of RBII depends on the GMF. The increase in the number of RBII corresponds to the periods of the sector structure domination in cycles 23 and 24.

RBIIs can be separated into two classes depending on the RBII end frequency. The cycle evolution and parameter interrelations are different for the RBIIs of different classes.

The different groups of RBII were also revealed depending on the GMF strength. RBIIs fall into three groups depending on the GMF strength. The first type RBIIs are associated with magnetic fields in the range of ≈0–2.5 μT, the second type RBIIs are associated with the GMF in the range of ≈3.5–5 μT, and the third type RBIIs are associated with the GMF in the range of ≈5.5–8.5. These groups are coincide for P1 and P2 RBIIs. Cycle 24 RBIIs are concentrated to the 0–5 μT GMF.

There is no unambiguous dependence between the RBII parameters. The interrelations between the different class RBII parameters are also different. All interrelations between RBII parameters are non-linear and are fairly widespread. Whereas, the frequency of a burst is a function of the plasma density in the RBII generation region, we can draw the conclusion, that RBIIs with the same parameters can be produced in the solar atmosphere regions under absolutely different plasma conditions. It suggests that their generation sources are different. It could also indicate that the mechanisms of RBII generation may be different.

Acknowledgements

The WIND/WAVES-STEREO RBII catalog at *http* : *//lep*694.*gsfc.nasa.gov/waves /data_products.html* was used.

Wilcox Solar Observatory data used in this study was obtained via the web site $http://wso.stanford.edu$ at $2015:02:26_00:54:03$ PST courtesy of J.T. Hoeksema. The Wilcox Solar Observatory is currently supported by NASA.

National Geophysical Data Center (USA) data on Wolf sunspot numbers were used.

References

Altschuler M.D., Newkirk G. (1969) Solar Phys. 9, 131
Altschuler M.D., Trotter D.E., Newkirk G.Jr., Howard R. (1975) Solar Phys. 41, 225
Altschuler M.D., Levine R.H., Stix M., Harvey J. (1977) Solar Phys. 51, 345
Bastian, T.S. (2007) ApJ 665, 805
Bilenko I.A. (2012) G&A 52, 1005
Bilenko I.A. (2013) IAU Sump. 300, 153
Bilenko I.A. (2014) Solar Phys. 289, 4209
Bilenko I.A. (2015) G&A 55, 1141
Bougeret J.L, Kaiser M.L., Kellogg P.J. et al. (1995) Space Sci. Rev. 71, 231
Bougeret J.L., Goetz K., Kaiser M.L., t al. (2008) Space Sci. Rev. 136, 487
Chernov G.P., Stanislavsky A.A., Konovalenko A.A. et al. (2007) AstL 33. 192 (PAZh 33, 221)
Cho K.-S., Gopalswamy N., Kwon R.-Y., et al. (2013) ApJ 765, 148
Cho, K.-S., Lee, J., Moon, Y.-J., et al. (2007) A&A 461, 1121
Cliver E.W., Web D. F., Howard R. A. (1999) Solar Phys. 187, 89
Cunha-Silva R.D., Fernandes F.C.R., Selhorst C.L. (2015) A&A 578, 7
Dodge J.C. (1975) Solar Phys. 42, 445
Gopalswamy N., Aguilar-Rodriguez E., Yashiro S., et al. (2005) JGR 110, S07
Gopalswamy N., Yashiro S, Akiyama S., et al. (2008) Ann. Geophys. 26, 3033
Gopalswamy N., Thompson W.T., Davila J.M., et al. (2009) Solar Phys. 259, 227
Hoeksema J.T. (1984) Ph. D. Thesis
Hoeksema J.T., Scherrer P.H. (1986) Solar Phys. 105, 205
Korolev O.S., Markeev A.K., Fomichev V.V., Chertok I.M. (1974) Sov. Astron. 17, 776
Kuckes A.F., Sudan R.N. (1971) Solar Phys. 17, 194
Makarov V.I., Sivaraman, K.R. (1989) Solar Phys. 123, 367
Makarov V.I., Tlatov A.G., Callebaut D.K.,Obridko V.N., Shelting B.D. (2001) 198, 409
Melrose D.B. (1980) Space. Sci. Rev. 26, 3
Payne-Scott R., Yabsley D.E., Bolton J.G. (1947) Nature 160, 256
Pohjolainen S., Allawi H., Valtonen E. (2013) A&A 558, A7
Sheeley Jr., N.R., Howard, R.A., Michels, D.J., et al. (1984) ApJ 279, 839
Vasanth V., Umapathy S. (2014) Journal of Astrophysics ID 168718
Vrsnak B., Aurass, H., Magdalenic, J., Gopalswamy, N. (2001) A&A 377, 321
Vrsnak, B., Warmuth, A., Temmer, M. (2006) A&A 448, 739
Wild J.P., McCready L.L. (1950) AJSRA 3, 541